Regulatory Roles of Differentially Expressed MicroRNAs in Metabolic Processes in Negative Lens-Induced Myopia Guinea Pigs

Dadong Guo
Eye Institute of Shandong University of Traditional Chinese Medicine
Meihua Ding
Affiliated Eye Hospital of Shandong University of Traditional Chinese Medicine
Xiaoli Song
Shandong University of Traditional Chinese Medicine
Yuanyuan Sun
Shandong University of Traditional Chinese Medicine
Guoping Li
Affiliated Eye Hospital of Shandong University of Traditional Chinese Medicine
Wanli Hu
Shandong University of Traditional Chinese Medicine
Zonghong Li
Shandong University of Traditional Chinese Medicine
Jianfeng Wu
Shandong University of Traditional Chinese Medicine
Wenjun Jiang
Eye Institute of Shandong University of Traditional Chinese Medicine
Hongsheng Bi (azuresky1999@163.com)
Affiliated Eye Hospital of Shandong University of Traditional Chinese Medicine https://orcid.org/0000-0002-1712-0055

Research article

Keywords: lens-induced myopia; microRNA profiling; guinea pig; peroxisome proliferator-activated receptor α; metabolic pathway

Posted Date: September 8th, 2019

DOI: https://doi.org/10.21203/rs.2.14110/v1

Version of Record: A version of this preprint was published on January 6th, 2020. See the published version at https://doi.org/10.1186/s12864-020-6447-x.

Abstract

Background: Myopia is the most common vision defects and the leading cause of visual impairment worldwide. microRNAs can regulate the target gene expressions, influencing the development of diseases. However, the roles of differentially expressed microRNAs in the development of myopia in lens-induced myopia (LIM) guinea pigs remain still unclear. Methods: We first established a negative LIM guinea pig model after induction for 2 weeks. Further, we isolated sclera to purify total messenger RNA (mRNA) in both LIM and LIM fellow sclera. Using next generation sequencing technique and bioinformatics analysis, we identified the differentially expressed microRNAs in LIM guinea pigs, performed the bioinformatics annotation for the differentially expressed microRNAs, and validated the expressions of differentially expressed microRNAs. Results: We successfully established a negative LIM model in guinea pigs, identified 27 differentially expressed microRNAs in LIM guinea pig sclera, including 10 up-regulated and 17 down-regulated microRNAs. The KEGG annotation showed the main signaling pathways were closely associated with PPAR signaling, pyruvate and propanoate metabolisms, and TGF-beta signaling pathways. Conclusions: In summary, we found the development of myopia is mainly involved in the disorder of metabolic processes in LIM guinea pigs. The PPAR signaling, pyruvate and propanoate metabolism pathways may play a role in the development of myopia.

Background

Myopia (short-sightedness) is the most common refractive error of the eye, and one of the leading cause of visual impairment worldwide (Tkatchenko et al. 2015) Other than causing blurred vision at distance, high myopia (excessive amount of myopia) exaggerates the risk of other ocular diseases including cataract, glaucoma, retinal detachment, and myopic degeneration, all of which can lead to irreversible vision loss (Wong et al. 2014). The economic burden mainly caused by myopia is up to US$ 202 billion per year (Smith et al. 2009) and by 2050, 50% and 10% of the world population is estimated to have myopia and high myopia, respectively (Holden et al. 2016). Both children and adults can be affected by myopia. However, it is often diagnosed in school-age children. In East Asia, more than 80% of high school graduates are subjected to have myopia, approximately 20% of which possess high myopia (Wu et al. 2013; Jonas et al. 2016; Ding et al. 2017). Usually, the younger the children's age at the beginning of myopia is, the more rapidly the condition will get worse and likelihood of developing a sight-threatening complication of high myopia will increase (Janowski et al. 2015) Physiologically, the occurrence of myopia is closely correlated with the axial elongation of the eye, and high myopia is characterized by scleral thinning and localized ectasia of the posterior sclera (Rada et al. 2006; Verkicharla et al. 2015).

The sclera is a dense, fibrous, and viscoelastic connective tissue that defines the size and shape of the eye. It can provide a strong framework which supports the retina, withstands the expansive force generated by intraocular pressure and provides an approach for aqueous outflow and protects the contents of the eye from external trauma (McBrien et al. 2003; Harper et al. 2015). Hence, the sclera is critical in determining the absolute size of the eye and thus plays an important role in determining the refractive state of the eye. To date, both experimental outcomes and clinical evidence have confirmed

that excessive ocular elongation related to myopia is attributed to altered extracellular matrix (ECM) remodeling of the scleral shell (Harper et al. 2015). The sclera undergoes a series of structural changes including marked thinning, reduction in collagen fibril diameter and fiber dysregulation that are the result of altered metabolism, ultimately leading to excessive axial elongation of the eye and visual impairment (McBrien et al. 2013). Moreover, modern theories of refractive development acknowledge the critical role of the sclera in the control of eye size and the development of myopia. During the development of myopia, both axial length and optical power of the eye increases, making the refractive error more negative (Mutti et al. 2007). Moreover, scleral extracellular matrix degrades, and the sclera becomes thinner (McBrien et al. 2013). Therefore, the development of myopia is closely associated with scleral remodeling. Nevertheless, which factors regulate this process is still unknown.

MicroRNAs (miRNAs) are a class of short, noncoding RNA molecules that can regulate messenger RNA (mRNA) at a posttranscriptional level by binding principally to the 3' untranslated regions (3'UTR) of specific mRNAs so as to silence gene expression or to promote degradation of target mRNAs (Ambros 2001; Ambros 2004). Thus, recognition of differentially expressed miRNAs will contribute to the understanding of disease progression, uncovering the pathogenic role of miRNAs. Previous studies have revealed that some diseases are closely related to the abnormal expression and regulation of miRNA-targeted mRNAs (Guo et al. 2015; Razzak et al. 2016; Irmak-Yazicioglu et al. 2016). It is reported that some miRNAs show age-related differential regulation, higher levels in the sclera of rapidly growing fetal eyes, and thus playing a role in ocular growth regulation (Metlapally et al. 2013) retinoic acid could also up-regulate miR-328 expression to control myopic development, indicating that miRNAs can represent potential targets for ocular growth manipulation, influencing the development of myopia (Chen et al. 2012) So far, the detailed mechanism of myopia development involved in miRNA regulation is still unclear.

In order to understand the underlying mechanism of myopia development, we used the guinea pig (*Cavia porcellus*, English short-hair stock, tricolor strain) as a mammalian model for myopia and established a negative lens-induced myopia (LIM) guinea pig model, identified the differentially expressed miRNAs in guinea pig sclera, and performed the related bioinformatics annotation. Our findings will provide new insights into the understanding of the biological process of myopia development.

Methods

Experimental overview

An overview of the general experimental procedures and workflow steps was provided in Figure 1.

Animals

Male guinea pigs (*Cavia porcellus*, English short-hair stock, tricolor strain, 3-week-old) of specific pathogen-free grade were purchased from Jinan Xilingjiao Laboratory Animal Co., Ltd. (Jinan, China). Four or five guinea pigs were raised together in a transparent plastic cage (20 × 30 × 35 cm). All guinea

pigs were fed and maintained under light/dark cycles of 12h/12h and were allowed access to food and water freely. Experiments were approved by the Institutional Animal Care and Use Committee of Shandong University of Traditional Chinese Medicine (20150103), and were strictly followed by the guidelines of Care and Use of Laboratory Animals published by China National Institute of Health and the ARVO Statement for the Use of Animals in Ophthalmic and Vision Research. Moreover, we ensure that our manuscript reporting adheres to the ARRIVE guidelines (http://www.nc3rs.org.uk/page.asp?id=1357) for the reporting of animal experiments.

Determination of Refraction

Streak retinoscopy and A-scan ultrasonography were applied to determine the related parameters associated with refraction status before and after induction of experimental myopia with -10D lens. The refraction of the eyes was defined as the mean value of the refractive errors along the vertical and horizontal meridians of 3 repeated measurements (McFadden et al. 2004; Lu et al. 2006).

Measurements of anterior chamber depth, axial length, crystalline lens thickness and vitreous length of guinea pigs were performed by A-scan ultrasonography (Cinescan, Quantel Medical, France). Results were obtained from the mean value of 10 repeated measurements to minimize the error. All these procedures were performed by the same professional optometrist.

Establishment of the negative lens-induced myopia (LIM) model

Sixty male guinea pigs were randomly divided into 2 groups: a normal control group and an LIM group. Each group contained 30 guinea pigs. Before induction of myopia, the related parameters related to refraction status were measured to exclude the congenital myopia. In LIM group, the right eyes for every guinea pig were covered with -10 D lens every day, while the LIM fellow eyes were covered with plano lens. The duration of the LIM model was maintained for 2 weeks. To ensure the effectiveness of the LIM model in guinea pigs, all lenses were cleaned every morning and evening. At the indicted time point, the related parameters of guinea pigs in both control and LIM groups were measured using streak retinoscopy and A-scan ultrasonography, respectively.

Haematoxylin and eosin (H&E) staining

After induction of myopia, guinea pigs in normal control and LIM groups were euthanized by intraperitoneal injection of 3% pentobarbital and all eyes were collected (n=6 for each group). After fixation in 4 % paraformaldehyde in 0.1 mol/L of phosphate-buffered saline (PBS; pH = 7.4) at 4°C for 24 h, sections were cut into 4 μm and then stained with H&E solution. The observation was done under an optical microscope (Eclipse 55i, Nikon, Japan). The image resolution was set to 2560 × 1920 pixels and posterior scleral thickness was measured using NIS elements D 3.2 software (Nikon, Japan).

Preparation of RNA, library construction and sequencing

For LIM guinea pigs, 6 guinea pigs were divided into 3 groups and each group included 2 subjects. After induction of myopia, LIM guinea pigs were euthanized under anaesthesia to isolate sclera. Sclera of both LIM and LIM fellows in each group was pooled, respectively. Further, sclera was then grinded under liquid nitrogen, and total RNA was purified using TRIzol reagent (Invitrogen, Carlsbad, CA). Bothe RNA quantity and purity were determined using a micro spectrophotometer (K5600, Beijing Kaiao Technology Development Co., Ltd., Beijing, China).

For preparation of sequencing library, total RNA from each sample was sequentially ligated to 3' and 5' small RNA adapters. Further, cDNA was synthesized and amplified using Illumina's proprietary RT primers and amplification primers. Subsequently, about 125-145 bp PCR amplified fragments were extracted and were purified on Novex 15% PAGE gel. Finally, the completed libraries were quantified by Agilent 2100 Bioanalyzer (Agilent Technologies, Palo Alto, CA).

In order to prepare cluster generation, samples were diluted to a final concentration of 8 pmol/L and then cluster generation was performed on the Illumina cBot using a TruSeq Rapid SR cluster kit (#GD-402-4001, Illumina). In the present study, high through-put sequencing was performed on Illumina HiSeq 2000 using TruSeq Rapid SBS kits (#FC-402-4-2, Illumina). All procedures were strictly followed by the manufacturer's instructions.

Raw data processing and predication of miRNAs

Raw sequences were generated as clean reads from Illumina HiSeq by real-time base calling and quality filtering. The clean reads were recorded in FASTQ format, containing the read information, sequences and quality encoding. Further, the 3' adapter sequence was trimmed from the clean reads. The reads with lengths shorter than 15 nt were discarded. As the 5'-adaptor was also used as the sequencing primer site, the 5'-adaptor sequence is not present in the sequencing reads. The trimmed reads were recorded in FASTA format and the length more than 15 nt was aligned to the pre-miRNA in miRBase 21 using Novoalign software.

Selection of differentially expressed miRNAs

All values of LIM and normal control eyes were statistically analyzed compared with those of the fellow eyes using a paired sample t-test. When compared the samples of profile differences, the "fold change" and P-value between LIM and fellow eyes were computed. The miRNA was excluded if the tag-count was less than 10. Those who had fold changes either >= 1.3 or <=0.76, P-value <= 0.05 were selected as the differentially expressed miRNAs in LIM subjects.

Validation of differentially expressed miRNAs by quantitative PCR (qPCR)

In this section, another six pairs of subjects were fabricated and were used to validate the differentially expressed miRNAs. Based on the results what we selected as the differentially expressed miRNAs (Table 1), six miRNAs including three up-regulated miRNAs (i.e., cavPor3-miR-novel-chrscaffold_128_37706, cavPor3-miR-novel-chrscaffold_76_32980, cavPor3-miR-novel-chrscaffold_107_36268) and three down-

regulated miRNAs (i.e., cavPor3-miR-novel-chrscaffold_13_13335, cavPor3-miR-novel-chrscaffold_119_37316, cavPor3-miR-novel-chrscaffold_120_37436) were randomly selected to be performed qPCR test. 5S rRNA was as an endogenous control. Briefly, total miRNAs were collected after purification from the pooled sclera using the RNAmisi microRNA Extraction Kit (Aidlab Biotechnologies Co., Ltd, Beijing, China). cDNA synthesis was performed using Invitrogen Superscript ds-cDNA synthesis kit in accordance with the manufacturer's instructions. qPCR determinations were done using miScript SYBR-Green PCR Kit (Qiagen) and the primers were provided in table 2. The reactions were incubated in a 384-well optical plate at 95 °C for 10 min, followed by a 40-cycle for 10 sec at 95 °C, 60 sec at 60 °C. Analysis was carried out in triplicate for each sample and repeated three times. Melting curve analysis (10 sec at 95 °C, 60 sec at 60 °C, and 15 sec at 95 °C) was used to confirm the specificity of the amplification reactions. 5S rRNA was used as the normalized control. The miRNA level was quantified using ABI PRISM 7900 system (Applied Biosystems, Foster City, CA, USA), and the relative expression of each miRNA was calculated using the $2^{-\Delta\Delta ct}$ method.

Target mRNA prediction

To further explore the potential biological function and biological processes of differentially expressed miRNAs, potential targets for miRNA action were predicted by using putative targets that generated from the relevant algorithms. Considering that there is no database for guinea pig miRNAs, we selected the database related to rat as target candidates according to the literature (Shan et al. 2013; Kuang et al. 2017). A combinatorial strategy was used where target miRNAs were predicted for the differentially expressed genes using three algorithms, i.e., mirbase (http://www.mirbase.org/), miRanda (http://www.microrna.org/) and miRDB (http://mirdb.org/miRDB/). The selection of predicted target mRNA was adopted using the overlapping from any two algorithms mentioned above.

Gene ontology (GO) function annotation

In accordance with the result of bioinformatics annotation, target mRNAs regulated by differentially expressed miRNAs in guinea pigs were picked out. These target genes were arrowed down using the UniGene database which is specific to enterology. GO function annotation was used to organize genes into hierarchical categories and uncover the miRNA-mRNA regulatory network based on the biological process and molecular function (Gene Ontology Consortium 2008). Both two-sided Fisher's exact test and $\chi 2$ test were used to classify the GO category. Meanwhile, false discovery rate (FDR) was used to calculate the P-value to correct the type I error rate. Herein, we selected a *P* value of <0.05 for both GOs and FDR.

KEGG pathway enrichment analysis

In the present study, the predicted target genes were classified according to Kyoto Encyclopedia of Genes and Genomes (KEGG) pathway annotations to identify the possible pathways that were actively regulated by differentially expressed miRNAs. These differentially expressed miRNA targets were collected and were carried out by KEGG pathway annotation (http://www.genome.jp/kegg/). A two sided Fisher's exact

test and χ2 test were used to classify the enrichment (Re) of pathway category. The FDR was calculated to correct the P-value of the type I error rate. The enrichment Re was obtained by the same formula that used in GO analysis. We selected the pathways that had a *P*-value of <0.05 and an FDR of <0.05. The regulator pathway annotation was also done based on the scoring and visualization of the pathways collected in the KEGG database (http://www.genome.jp/kegg/).

Validation of PPAR-α by Q-PCR and western blotting

In view of the result of KEGG pathway enrichment analysis, we selected peroxisome proliferator-activated receptor (PPAR) α, predicted as a down-regulated gene in guinea pig sclera under the LIM condition and regulated by cavPor3-miR-novel-chrscaffold_128_37706, to validate the expression at both mRNA and protein levels. For qPCR analysis of PPAR α mRNA level, total RNA (n=6 for each group) was extracted from both LIM guinea pig sclera and normal control subjects using TRIzol reagent (Invitrogen Life Technologies, Gaithersburg, MD). After analyses of RNA concentration and purity, the first-strand cDNA was synthesized using 1 μg of total RNA. The qPCR reaction was performed using LightCycler 480 SYBR Green I Master (Roche Diagnostics, IN, USA) in a 20 μl volume. The PCR reaction program was performed by a LightCycler 480 II (Roche Diagnostics GmbH, Mannheim, Germany) with an initial denaturation of 95 °C for 5 min, followed by 45 cycles of 95 °C for 20s, 58 °C for 20 s and 72 °C for 25 s. The △△CT values of relative gene levels were calculated as fold change in mean ± standard error (SD) after normalization to respective endogenous β-actin control. The primers were as follows: β-actin: forward: 5'-accccaaggccaaccgtgagaagatg-3', reverse: 5'-ctcggccgtggtggtgaaactgtagc-3'; PPAR α: forward: 5'-tcaaaaacctccgcaaacccttct-3', reverse: 5'-ggccgatctccgcagcaaatga-3'.

Moreover, we also performed western blotting to determine the alterations of PPAR α protein before and after induction of myopia in guinea pig sclera. Briefly, pooled sclera samples (n=6 for each group, 15 μL/lane) in both LIM and normal control subjects were loaded onto 12% sodium dodecyl sulfate (SDS)-polyacrylamide gel electrophoresis (SDS-PAGE), and run for 90 min at 100 V, then the isolated proteins were transferred to poly (vinylidene) fluoride (PVDF) membrane (Millipore) at 100 V for 120 min, and then membranes were blocked in TBST (5% skim milk in 0.05% Tween 20 in TBS) buffer for 1 h at room temperature, followed by five washes with TBST for 5 min. Membranes were then incubated with rabbit polyclonal antibody against PPAR α (1:400, Abcam, Cambridge, UK) overnight at 4 °C. The membranes were washed five times with TBST for 5 min each and incubated with horseradish peroxidase-labeled anti-rabbit secondary antibodies (Amersham Biosciences Co., Piscataway, NJ) diluted in 5% non-fat dry milk in TBST (1:2000) for 1 h at room temperature. Next, the membrane was washed one time in TBST for 10 min followed by 2 washes for 5 min each. Finally, visualization was performed with DAB (Sigma) using the FUSION-FX7 imaging system (Vilber Lourmat Lourmat, Marne-la-Vallée, France) and quantified by Fusion CAPT Software (Vilber Lourmat, France). Meanwhile, anti-beta actin (1:2000, Abcam, Cambridge, UK) was used as an internal loading control. The ratio of PPAR α to actin was used to standardize across samples.

Both qPCR and Western blotting experiments were repeated 3 times, the values were presented as mean ± SD (standard deviation).

Luciferase-reporter activity assay

According to the manufacturer's instructions, the products were cloned into pmiR-RB-REPORTTM vectors (Ribio Biotech, Guangzhou, China) downstream from the hRluc luciferase coding sequence. First, primers of both wild type and mutant type of PPAR α were synthesized. The primer sequences were as follows: forward primer of wild type: GCGGCTCGAGATTTTTCCTGAGATGGTAG, reverse primer of wild type: AATGCGGCCGCCCTGTAATTGTCTGAATCC; forward primer of mutant type: AGCAGGGAAAACGTGTGATGGCCTCCCTCCTTAC, reverse primer of mutant type: AGGCCATCACACGTTTTCCCTGCTCTCCTGTATG. The qPCR amplification of target gene was performed using a LightCycler 480 II (Roche Diagnostics GmbH, Mannheim, Germany). Next, cells were co-transfected with 40 ng of 3'-UTR reporter constructs containing either wild-type or mutated binding sites and 100 nM of miR-novel-chrscaffold_128_37706 mimic or negative control into 293T cells using Lipofectamine 2000 (Invitrogen, USA). After 48 h of transfection, luciferase activity was measured using a Dual-Luciferase Reporter Assay System Kit (Promega Biotech, Madison, WI, USA). The activities of hRluc were first normalized to the internal control (hluc) to evaluate the transfection efficiency. Further, the firefly luciferase activity was normalized to Renilla activity, which was used as an internal control. The experiments were repeated three times, and the result was presented as mean ± SD.

Statistical analysis

Statistical analysis was carried out using the SPSS statistical software (SPSS Version 17.0, Chicago, USA). The results of LIM eyes were statistically compared with those of the fellow eyes within the same group using a paired sample t-test. Statistical analysis among groups was performed by one-way ANOVA. $P < 0.05$ was considered statistically significant.

Results

Alterations of axial length and refraction

Various parameters associated with refractive status, such as anterior chamber depth, axial length, crystalline lens thickness and vitreous length, were measured before and after myopia induction. As listed in Table 3, the results indicated that there was no significant difference in anterior chamber depth, crystalline lens thickness and vitreous length among all groups between normal control guinea pigs and LIM subjects before induction of myopia (all $P > 0.05$, one-way ANOVA). However, after myopia induction for 2 weeks, we observed that the vitreous length, axial length, and refraction markedly changed. The vitreous length and axial length were markedly elongated in LIM eyes as compared with those of fellow eyes, whereas the refraction of LIM eyes was significantly decreased as compared with that of LIM fellow eyes, and these alterations accompanied by significant differences between LIM eyes and LIM fellow eyes (a paired sample t-test, $P<0.0001$).

Alterations of posterior sclera in LIM eyes

Considering that thinned posterior sclera is an important event in the development of myopia (McBrien et al. 2013), we further explored the alteration of the thickness of posterior sclera in LIM guinea pigs. We observed that there was no significant alteration of the thickness in posterior sclera between normal left and right eyes (275.75±8.50 μm vs. 273.50±6.75 μm, $P>0.05$; a paired sample *t*-test), and there was also no marked change between normal and LIM fellow eyes (273.50±6.75 μm vs. 267.38±8.83 μm, $P>0.05$; independent samples *t*-test). However, the sclera of LIM eyes was significantly thinner (216.75±8.17 μm) compared with those of either LIM fellow eyes ($P<0.01$; a paired sample *t*-test) or normal eyes ($P<0.01$; independent samples *t*-test), accompanied by a statistical difference (Figure 2).

Differentially expressed miRNA profiling

The identification of miRNAs was performed by high-throughput sequencing data with an Illumina HiSeq 2000 platform and following prediction by algorithms. We found that 27 differentially expressed miRNAs in LIM guinea pig sclera were significantly altered at a fold change threshold of 1.3 and FDR corrected P-value threshold of 0.05. The differentially expressed miRNAs was presented as a volcano plot (Figure 3) and included 10 up-regulated and 17 down-regulated miRNAs (Table 1).

Validation of differentially expressed miRNAs

As shown in Figure 4, 6 miRNAs among these filtered ones were validated to be significantly differentially expressed in LIM guinea pig sclera versus fellow subjects, in which cavPor3-miR-novel-chrscaffold_128_37706 ($P<0.01$), cavPor3-miR-novel-chrscaffold_76_32980 and cavPor3-miR-novel-chrscaffold_107_36268 ($P<0.05$) were up-regulated miRNAs, whereas cavPor3-miR-novel-chrscaffold_119_37316, cavPor3-miR-novel-chrscaffold_13_13335 and cavPor3-miR-novel-chrscaffold_119_37316 were down-regulated miRNA ($P<0.05$), and these results were in agreement with those by sequencing and prediction by algorithms.

Gene ontology (GO) function annotation

In the present study, the pie chart showed the top ten counts of the significant enrichment terms in biological process and molecular function (Figure 5). Based on the annotation of biological process, the miRNA-targeted genes were classified into 1108 categories, including cellular process, single-organism process, single-organism cellular process, biological regulation and metabolic process, while 4847 categories were involved in binding, protein binding, and organic cyclic compounding binding.

KEGG pathway enrichment analysis

Based on the sequencing data and following prediction by algorithms, the differentially expressed miRNAs in guinea pig sclera were identified. The KEGG function annotation was performed based on the putative target genes that were regulated by miRNAs. All predicted targets were clustered into 42 pathways for miRNA targeted genes. Among all these differentially regulated signaling pathways, the

main pathways were PPAR signaling, pyruvate metabolism, propanoate metabolism, ascorbate and aldarate metabolism, glycolysis/gluconeogenesis, GABAergic synapse and TGF-beta signaling pathways (Figure 6).

Expressions of PPAR-α

The expressions of PPAR-α at both mRNA and protein levels were explored by using qPCR and western blot techniques. As shown in Figure 7, the results indicated that there was no difference between the two eyes in normal control subjects. However, after induction with negative lens for 2 weeks, apparent statistical difference was observed between LIM and LIM fellow eyes. Nevertheless, there was no statistical difference between LIM fellow eyes and normal control subjects. However, significant statistical difference was observed between LIM eyes and both normal control subjects at mRNA and protein levels (Figure 7A, C).

Dual-luciferase reporter assay

We also performed a dual-luciferase reporter assay to validate whether cavPor3-miR-novel-chrscaffold_128_37706 regulates the expression of PPAR-α mRNA. The result demonstrated that the relative luciferase activity of the negative control group with wild-type carriers was 1.00 ± 0.062. It was 0.646 ± 0.042 and 1.00 ± 0.023 for the cavPor3-miR-novel-chrscaffold_128_37706 group with wild-type carriers and the negative control group with mutant carriers, respectively. Regarding the cavPor3-miR-novel-chrscaffold_128_37706 group with mutant carriers, the relative activity was 1.053 ± 0.006 (Figure 8). These data suggest that cavPor3-miR-novel-chrscaffold_128_37706 (i.e., miR-19b-3p) may specifically regulate PPAR-α expression by targeting UUUGCACA at the 3'-UTR.

Discussion

The development of myopia is a complicated process which involves the participation of many molecules and signaling pathways. Currently, some investigations of animal models have permitted tests of hypothesis as to myopia's origins, indicating that normal growth of the eye is related to the roles of lower vitamin D levels, peptide factors, metabolism and accommodation (Lieberman et al. 1991; Yazar et al. 2014).

Studies have shown that the scleral remodeling and the consequent alteration of axial length are closely correlated with the development of myopia. The longer the axial length is, the more severe the myopia becomes (Kimura et al. 2007). To date, lens induction can efficiently disrupt the normal growth process, and induce rapid axial elongation, leading to the occurrence of myopia. It was reported that a negative lens-induced myopia model is a more credible model than that of form-deprivation myopia for the study of juvenile-onset myopia (Ganesan et al. 2010), and the guinea pig is considered to be a suitable alternative for the mammalian model of lens-induced myopia (Xiao et al. 2014). Thus, we selected the LIM guinea pig model to investigate the possible mechanism in the development of myopia. In the present study, we have successfully established a negative LIM model in guinea pigs, and noted the

successful LIM model accompanied by apparent elongated axial length, vitreous length and reduced refraction (Table 3). We also found that there is change in the crystalline lens thickness (Table 3). It is noted an increase from 3.39mm to 3.61mm in the fellow eye and 3.41mm to 3.63mm in the LIM eye. Therefore, the changes in the refractive error cannot only be attributed to increase in vitreous chamber depth and scleral thinning. The change in axial length also includes increased lens thickness. Meanwhile, the decreased thickness in posterior sclera also occurred in LIM eyes (Figure 2), indicating that the development of myopia is involved in the scleral remodeling.

MiRNAs play important roles in the regulation of gene expression in many biological and pathological processes including cell proliferation, differentiation, apoptosis and stress response (Dong et al. 2013). Hence, identification of differentially expressed miRNAs will facilitate the understanding of the development and pathogenesis of diseases. In order to further explore the role of miRNAs in the development of myopia, we investigated the alteration of miRNA profiling in LIM guinea pig sclera. After induction of experimental myopia with negative lens for two weeks, we identified the differentially expressed miRNAs in LIM sclera in a guinea pig model. The results showed that there were 27 differentially expressed miRNAs in LIM guinea pig sclera. Subsequent bioinformatics analysis of GO annotation demonstrated that the genes targeted by differentially expressed miRNAs were mainly associated with cellular, single-organism, biological, metabolic and organic substance metabolic processes (Figure 5), indicating the development and pathogenesis of experimental myopia involve the participation of multiple biological processes and molecules; that is to say, a lot of genes are closely related to the development of pathogenesis of myopia. The developmental process of myopia may be correlated with the scleral remodeling and the regulation of axial length (Guo et al. 2014). Similarly, 75 miRNAs with differential expressions from the whole eye, retina and sclera were identified in form-deprivation induced myopia mice, and the differentially expressed miRNAs are associated with cell pluripotency maintenance, growth and development regulation, indicating that miRNAs play important roles in the developmental and regulatory roles in eye growth (Luo et al. 2013). Metlapally et al. observed the increased expression of mir-214, let-7c, let-7e, mir-103, mir-107, and mir-98 in fetal sclera (Metlapally et al. 2013), and differing in our investigations. This difference may be due to the different species, and the differentially expressed miRNAs in fetal sclera is congenital, whereas our results were obtained from a negative LIM model. Moreover, using microarray technology, Tkatchenko and colleagues explored myopia-associated miRNA expression profiling in both retina and sclera of C57Bl/6J mice with form-deprivation myopia. They found a total of 53 differentially expressed miRNAs in the retina and no differences in miRNA expression in the sclera of mice. They noted that the differentially expressed miRNAs-targeted genes are mainly associated with transcription factors and/or regulatory proteins (Tkatchenko et al. 2016). Mei and colleagues explored the differentially expressed miRNAs in form-deprived myopia in sclera of C57Bl/6J mice. They found 8 differentially expressed miRNAs and enriched 1,805 target genes. The functionally collaborative network revealed that "regulation of transcription" was significantly enriched. KEGG pathway analysis further revealed that "Axon guidance" and "TGF-β signaling pathway" were involved in the development of myopia of mice (Mei et al. 2017). In our study, we only investigated the miRNA expression profiling in sclera of LIM guinea pigs. We noted that the

differentially expressed miRNAs-targeted genes were closely associated with cellular process, PPAR signaling pathway, pyruvate metabolism, and TGF-β signaling pathway. The differences may be attributed to the different species and modeling methods. Form deprivation and negative lens-induced myopia have been widely applied in the study of the visual regulation of eye growth. Although their similar outcomes of excessive eye elongation and myopia, the visual stimuli differ: form deprivation provides no visual feedback and so constitutes an open-loop system, whereas negative lens-induced myopia provide a focal plane, and so is closed-loop (Nickla et al. 2015).

Homeodomain-interacting protein kinase 2 (HIPK2) is a conserved serine/threonine kinase. It can regulate transcription, cell differentiation, proliferation and apoptosis. Epithelial-mesenchymal transition (EMT) plays a critical role in embryonic development, wound healing, tissue regeneration and organ fibrosis. It is reported that miR-141, a member of the miR-200 family, can inhibit EMT, and regulate renal fibrosis via TGF-β1/miR-141/HIPK2/EMT axis (Huang et al. 2015). In our study, we noted that cavPor3-miR-novel-chrscaffold-107-36268, an up-regulated miRNA, is miR-141-3p. Considering that the fibrosis of sclera plays an important role in scleral remodeling and further influence the development of myopia, we speculate that up-regulated cavPor3-miR-novel-chrscaffold-107-36268 may regulate the development of myopia via TGF-β signaling pathway, and this result is also in agreement with that of KEGG pathway enrichment analysis (Figure 6).

PPARs are nuclear receptors that are closely associated with the thyroid hormone and retinoid receptors, which function as regulators of lipid and lipoprotein metabolism and glucose homeostasis, influencing cell proliferation, differentiation, apoptosis, and inflammation (Zolezzi et al. 2013; Tanaka et al. 2014). In our study, we found that cavPor3-miR-novel-chrscaffold-128-37706 is miR-19b-3p, and it may be a potential direct regulator of PPAR α. In order to investigate whether cavPor3-miR-novel-chrscaffold-128-37706 regulates the expression of PPAR α, we performed dual-luciferase reporter assay, and found that PPAR α is the target gene regulated by cavPor3-miR-novel-chrscaffold-128-37706, indicating that cavPor3-miR-novel-chrscaffold-128-37706 can play a role in PPAR signaling pathway, and thus influence the development of myopia.

Moreover, the result of the KEGG pathway enrichment analysis indicates that the differentially expressed miRNAs mainly involve PPAR signaling pathway, pyruvate metabolism, propanoate metabolism, ascorbate and aldarate metabolism, glycolysis/gluconeogenesis, GABAergic synapse, TGF-β signaling pathway (Figure 6). That is to say, the myopic development may be correlated with the metabolic imbalance. To validate the predicated molecules of KEGG pathway enrichment analysis, we determined the PPAR α expressions at both RNA and protein levels. Our results showed that PPAR α expression were reduced significantly in LIM guinea pig sclera compared with that in LIM fellow subject (Figure 7), indicating that PPAR signaling pathway is related to the development of myopia in LIM guinea pigs.

Bertrand and colleagues found that in chicken with experimental myopia model, peroxisome proliferator-activated receptor α agonist GW7647 can result in an up-regulation of apoA-I level and in a significant

reduction of experimental myopia (Bertrand et al. 2006). Thus, this result and our findings both demonstrate that PPAR signaling pathway may play a pivotal role in the development of myopia.

Nevertheless, potential limitations of our study should be mentioned. First, there has been no a complete bioinformatics database so far on guinea pigs, therefore, we performed the relative analysis by reference to the rat bioinformatics database. Second, the animals used for measurement of scleral tissue thickness and those used for RNA-sequencing were different, and the phenotyping was not done in the eyes that scleral tissue was extracted for sequencing; this may result in deviation of the outcome. Third, the development of myopia is involved in whole visual pathways, in order to completely address the underlying mechanism of myopia, systematic investigations should be further carried out.

Conclusions

The present work represents an initial study on the differentially expressed miRNA profile of the sclera in a lens-induced myopia guinea pig model versus normal control subjects. The differentially expressed miRNAs and the prediction of their target genes provide a basis for further understanding the role of miRNAs in LIM guinea pig sclera and the biological processes in which they are involved. The LIM guinea pig is a good model species for various biological studies in the development and pathogenesis of myopia, and our results indicate that the occurrence of the myopia is closely linked to the involvement of multiple signaling pathways including PPAR signaling pathway, pyruvate and propanoate metabolisms, GABAergic synapse, TGF-β and Jak-STAT signaling pathways, indicating that the occurrence of myopia may be closely related to metabolic processes. Taken together, our investigation provides a new insight into the mechanism of the occurrence and development of myopia.

Abbreviations

FDR: false discovery rate; GO: Gene ontology; H&E: Haematoxylin and eosin; KEGG: Kyoto Encyclopedia of Genes and Genomes; LIM: lens-induced myopia; mRNA: messenger RNA; miRNAs: MicroRNAs; PAGE: polyacrylamide gel electrophoresis; PBS: phosphate-buffered saline; qPCR: quantitative PCR; SD: standard deviation; SDS: sodium dodecyl sulfate

Declarations

Ethics approval and consent to participate

Experiments were approved by the Institutional Animal Care and Use Committee of Shandong University of Traditional Chinese Medicine (20150103), and were strictly followed by the guidelines of Care and Use of Laboratory Animals published by China National Institute of Health and the ARVO Statement for the Use of Animals in Ophthalmic and Vision Research. Moreover, we ensure that our manuscript reporting adheres to the ARRIVE guidelines (http://www.nc3rs.org.uk/page.asp?id=1357) for the reporting of animal experiments.

Consent to publish

Not applicable.

Availability of data and materials

The data used to support the findings of this study are available from the corresponding author upon request.

Competing interests

The authors declare no conflict of interest.

Funding

This study was supported by Key Development & Research Program of Shandong Province (2019GSF108252, 2016GGH3119, 2017CXGC1211) and National Natural Science Foundation of China (No. 81603421). The founding sponsors had no role in the design of the study, in the collection, analyses, or interpretation of data, in the writing of the manuscript, and in the decision to publish the results.

Authors' Contributions

DDG and HSB conceived and designed the study; YYS, XLS, WLH and ZHL performed the experiments; WJJ and JFW analyzed the data; MHD and GPL contributed reagents/materials/analysis tools; DDG and WJJ wrote the paper. All authors read and approved the final manuscript.

Acknowledgements

We thank Aksomics Inc. (Shanghai, China) for the assistance in performing analysis of bioinformatics.

References

Ambros V (2001) MicroRNAs: tiny regulators with great potential. Cell 107:823-826.

Ambros V (2004) The functions of animal microRNAs. Nature 431:350-355.

Bertrand E, Fritsch C, Diether S, Lambrou G, Müller D, Schaeffel F, Schindler P, Schmid KL, Van Oostrum J, Voshol H (2006) Identification of apolipoprotein A-I as a "STOP" signal for myopia. Mol Cell Proteomics 5:2158-2166.

Chen KC, HsiE, Hu CY, Chou WW, Liang CL, Juo SHH (2012) MicroRNA-328 may influence myopia development by mediating the PAX6 gene influence of microRNA-328 on myopia development. Invest Ophth Vis Sci 53:2732-2739.

Ding BY, Shih YF, Lin LL, Hsiao CK, Wang IJ (2017) Myopia among Schoolchildren in East Asia and Singapore. Surv Ophthalmol 62:677-697.

Dong H, Lei J, Ding L, Wen Y, Ju H, Zhang X (2013) MicroRNA: function, detection, and bioanalysis. Chem Rev 113:6207-6233.

Ganesan P, Wildsoet C F (2010) Pharmaceutical intervention for myopia control. Expert Rev Ophthalmol 5:759-787.

Gene Ontology Consortium (2008) The Gene Ontology project in 2008. Nucleic Acids Res 36:D440-444.

Guo D, Li J, Liu Z, Tang K, Song H, Bi H (2015) Characterization of microRNA expression profiling in peripheral blood lymphocytes in rats with experimental autoimmune uveitis. Inflamm Res 64:683-696.

Guo L, Frost MR, Siegwart JrJT, Norton TT (2014) Scleral gene expression during recovery from myopia compared with expression during myopia development in tree shrew. Mol Vis 20:1643.

Harper AR, Summers JA (2015) The dynamic sclera: extracellular matrix remodeling in normal ocular growth and myopia development. Exp Eye Res 133:100-111.

Holden BA, Fricke TR, Wilson DA, Jong M, Naidoo KS, Sankaridurg P, Wong TY, Naduvilath, T.J, Resnikoff S (2016) Global prevalence of myopia and high myopia and temporal trends from 2000 through 2050. Ophthalmology123:1036-1042.

Huang Y, Tong J, He F, Yu X, Fan L, Hu J, Tan J, Chen Z (2015) miR-141 regulates TGF-β1-induced epithelial-mesenchymal transition through repression of HIPK2 expression in renal tubular epithelial cells. Int J Mol Med 35:311-318.

Irmak-Yazicioglu MB (2016) Mechanisms of microRNA deregulation and microRNA targets in gastric cancer. Oncol Res Treat 39:136-139.

Janowski M, Bulte JW, Handa JT, Rini D, Walczak P (2015) Concise review: using stem cells to prevent the progression of myopia-a concept. Stem Cells 33: 2104-2113.

Jonas JB, Xu L, Wei WB, Wang YX, Jiang WJ, Bi HS, Panda-Jonas S (2016) Myopia in China: a population-based cross-sectional, histological, and experimental study. Lancet 388 Suppl 1:S20.

Kimura S, Hasebe S, Miyata M, Hamasaki I, Ohtsuki H (2007) Axial length measurement using partial coherence interferometry in myopic children: repeatability of the measurement and comparison with refractive components. Jpn J Ophthalmo 51:105-110.

Kuang L, Deng Y, Liu X, Zou Z, Mi L (2017) Differential expression of mRNA and miRNA in guinea pigs following infection with HSV2v. Exp Ther Med. 14(3):2577-2583.

Lieberman AR (1991) Myopia and the control of eye growth. J Neurocytol 20:856-856.

Lu F, Zhou X, Zhao H, Wang R, Jia D, Jiang L, Xie R, Qu J (2006) Axial myopia induced by a monocularly-deprived facemask in guinea pigs: A non-invasive and effective model. Exp Eye Res 82:628-636.

Luo X, Tkatchenko T, Tkatchenko A, Metlapally R, Gonzalez P, Young T (2013) Evaluation of microRNA expression profiles for form-deprivation myopia in mouse. Invest Ophth Vis Sci 54:3673-3673.

McBrien NA (2013) Regulation of scleral metabolism in myopia and the role of transforming growth factor-beta. Exp Eye Res 114:128-140.

McBrien NA, Gentle A (2003) Role of the sclera in the development and pathological complications of myopia. Prog Retin Eye Res 22:307-338.

McFadden SA, Howlett MH, Mertz JR. (2004) Retinoic acid signals the direction of ocular elongation in the guinea pig eye. Vision Res 44:643-653.

Mei F, Wang J, Chen Z, Yuan Z (2017) Potentially Important MicroRNAs in form-deprivation myopia revealed by bioinformatics analysis of microRNA profiling. Ophthalmic Res 57:186-193.

Metlapally R, Gonzalez P, Hawthorne FA, Tran-Viet KN, Wildsoet CF, Young TL (2013) Scleral micro-RNA signatures in adult and fetal eyes. PLoS One 8:e78984.

Mutti DO, Hayes JR, Mitchell GL, Jones LA, Moeschberger ML, Cotter SA, Kleinstein RN, Manny RE, Twelker JD, Zadnik K, CLEERE Study Group (2007) Refractive error, axial length, and relative peripheral refractive error before and after the onset of myopia. Invest Ophthalmol Vis Sci 48:2510-2519.

Nickla DL, Yusupova Y, Totonelly K (2015) The muscarinic antagonist MT3 distinguishes between form deprivation- and negative lens-induced myopia in chicks. Current Eye Research 40:1-6.

Rada JAS, Shelton S, Norton TT (2006) The sclera and myopia. Exp Eye Res 82:185-200.

Razzak R, Bédard ELR, Kim JO, Gazala S, Guo L, Ghosh S, Joy A, Nijjar T, Wong E, Roa WH (2016) MicroRNA expression profiling of sputum for the detection of early and locally advanced non-small-cell lung cancer: a prospective case-control study. Curr Oncol 23:e86-94.

Shan H, Zhang Y, Cai B, Chen X, Fan Y, Yang L, Chen X, Liang H, Zhang Y, Song X, Xu C, Lu Y, Yang B, Du Z (2013) Upregulation of microRNA-1 and microRNA-133 contributes to arsenic-induced cardiac electrical remodeling. Int J Cardiol. 167(6):2798-805.

Smith TS, Frick KD, Holden BA, Fricke TR, Naidoo KS (2009) Potential lost productivity resulting from the global burden of uncorrected refractive error. Bull World Health Org 87:431-437.

Tanaka S, Sugiyama N, Takahashi Y, Mantoku D, Sawabe Y, Kuwabara H, Nakano T, Shimamoto C, Matsumura H, Marunaka Y, Nakahari T (2014) PPARα autocrine regulation of Ca^{2+}-regulated exocytosis

in guinea pig antral mucous cells: NO and cGMP accumulation. Am J Physiol Gastrointest Liver Physiol 307:G1169-1179.

Tkatchenko AV, Luo X, Tkatchenko TV, Vaz C, Tanavde VM, Maurer-Stroh S, Zauscher S, Gonzalez P, Young TL (2016) Large-scale microRNA expression profiling identifies putative retinal miRNA-mRNA signaling pathways underlying form-deprivation myopia in mice. PloS One 11:e0162541.

Tkatchenko AV, Tkatchenko TV, Guggenheim JA, Verhoeven VJ, Hysi PG, Wojciechowski R, Singh PK, Kumar A, Thinakaran G, Williams C (2015) APLP2 regulates refractive error and myopia development in mice and humans. PLoS Genet 11:e1005432.

Verkicharla PK, Ohno-Matsui K, Saw SM (2015) Current and predicted demographics of high myopia and an update of its associated pathological changes. Ophthalmic Physiol Opt 35:465-745.

Wong TY, Ferreira A, Hughes R, Carter G, Mitchell P (2014) Epidemiology and disease burden of pathologic myopia and myopic choroidal neovascularization: an evidence-based systematic review. Am J Ophthalmol 157:9-25.

Wu JF, Bi HS, Wang SM, Hu YY, Wu H, Sun W, Lu TL, Wang XR, Jonas JB (2013) Refractive error, visual acuity and causes of vision loss in children in Shandong, China. The Shandong Children Eye Study. PLoS One 8:e82763.

Xiao H, Fan ZY, Tian XD, Xu YC (2014) Comparison of form-deprived myopia and lens-induced myopia in guinea pigs. Int J Ophthalmol 7:245-250.

Yazar S, Hewitt AW, Black LJ, McKnight CM, Mountain JA, Sherwin JC, Oddy WH, Coroneo MT, Lucas RM, Mackey DA (2014) Myopia is associated with lower vitamin D status in young adults myopia and vitamin D status. Invest Ophth Vis Sci 55:4552-4559.

Zolezzi JM, Inestrosa NC (2013) Peroxisome proliferator-activated receptors and Alzheimer's disease: hitting the blood-brain barrier. Mol Neurobiol 48:438-451.

Tables

Table 1 Differentially expressed miRNAs in negative lens-induced myopia guinea pig sclera versus fellow subjects

Mature-ID of miRNAs	Mature-sequence	Known name	Expressions
cavPor3-miR-novel-chrscaffold-107-36268	UAACACUGUCUGGUAAAGAUG	rno-miR-141-3p	Up
cavPor3-miR-novel-chrscaffold-111-36350	UUGUACAUAGUAGGCUUUCAUU	rno-miR-493-5p	Up
cavPor3-miR-novel-chrscaffold-4-5889	UUGGCUCUGCGAGGUCGGCU	rno-miR-1842	Up
cavPor3-miR-novel-chrscaffold-7-7504	CUGCGGUGAGCCUUGAAGCCU	--	Up
cavPor3-miR-novel-chrscaffold-111-36469	GAAUGUUGCUCGGUGAACCCCU	rno-miR-409	Up
cavPor3-miR-novel-chrscaffold-76-32980	CUAAGCCAGGGAUUGUGGGU	--	Up
cavPor3-miR-novel-chrscaffold-11-11041	UUUGGCAAUGGUAGAACUCACACU	rno-miR-182-5p	Up
cavPor3-miR-novel-chrscaffold-111-36611	UGGAUCUUUGUCACCAGCUGAACCU	--	Up
cavPor3-miR-novel-chrscaffold-132-37863	AAUGUACCUGGGCAAGGGUUC	rno-miR-500-3p	Up
cavPor3-miR-novel-chrscaffold-128-37706	UGUGCAAAUCCAUGCAAAACUG	rno-miR-19b-3p	Up
cavPor3-miR-novel-chrscaffold-10-11197	UAUUGCACUCGUCCCGGCCUCC	rno-miR-92b-3p	Down
cavPor3-miR-novel-chrscaffold-111-36353	UCCUAUAUGAUGCCUUUCCUC	--	Down
cavPor3-miR-novel-chrscaffold-111-36441	AAUCGUACAGGGUCAUCCACUU	rno-miR-487b-3p	Down
cavPor3-miR-novel-chrscaffold-15-15154	ACCGGGUGCUGUAGGCUU	--	Down
cavPor3-miR-novel-chrscaffold-12-12421	UGGAAUGUAAGGAAGUGUGUGG	rno-miR-206-3p	Down
cavPor3-miR-novel-chrscaffold-2-2212	GAGCAGGACGGUGGCCA	--	Down
cavPor3-miR-novel-chrscaffold-119-37316	UGGAAUGUAAAGAAGUGUGUAU	rno-miR-1-3p	Down
cavPor3-miR-novel-chrscaffold-111-36472	UGGUCGACCAGUUGGAAAGU	rno-miR-412-5p	Down
cavPor3-miR-novel-chrscaffold-68-31730	GUGCAUGAUGACAACUG	rno-miR-1341	Down
cavPor3-miR-novel-chrscaffold-84-33871	UGAUUGCAUCCUCUGAGGGAGA	--	Down
cavPor3-miR-novel-chrscaffold-128-37724	CAAAACGUGAGGCGCUGCUAU	--	Down
cavPor3-miR-novel-chrscaffold-120-37436	AAUGUGUAGCAGAAGACAGACU	--	Down
cavPor3-miR-novel-chrscaffold-46-27908	AAUGGCGCCACUAGGGUUGUGA	rno-miR-652-3p	Down
cavPor3-miR-novel-chrscaffold-27-20777	ACAGUAGUCUGCACAUUGGUU	rno-miR-199a-3p	Down
cavPor3-miR-novel-chrscaffold-13-13335	UUGGCCUACAGAAGUGACAGAC	--	Down
cavPor3-miR-novel-chrscaffold-84-33870	CAACUCCAGGAUUCGUCGAUC	--	Down
cavPor3-miR-novel-chrscaffold-26-19738	UUAUAAUACAACCUGAUAAGU	rno-miR-374a-5p	Down

Table 2 Primer sequences for differentially expressed miRNAs determined by quantitative PCR

Target gene name	Primers
5S rRNA	F: 5’TCTCGTCTGATCTCGGAAGC3’
	R: 5’GCGGTCTCCCATCCAAGTA3’
cavPor3-miR-novel-chrscaffold-13-13335	GSP: 5’CGATTCGTTGGCCTACAGAAGTG3’
	R: 5’ATCCAGTGCAGGGTCCGAGG3’
cavPor3-miR-novel-chrscaffold-120-37436	GSP: 5’CGCTCCGAATGTGTAGCAGAAGA3’
	R: 5’ATCCAGTGCAGGGTCCGAGG3’
cavPor3-miR-novel-chrscaffold-119-37316	GSP: 5’GGGGGTGGAATGTAAAGAAGT3’
	R: 5’GTGCGTGTCGTGGAGTCG3’
cavPor3-miR-novel-chrscaffold-128-37706	GSP: 5’GGGGTTGTGCAAATCCATG3’
	R: 5’GTGCGTGTCGTGGAGTCG3’
cavPor3-miR-novel-chrscaffold-107-36268	GSP: 5’CGCCATCGTAACACTGTCTGGTA3’
	R: 5’ATCCAGTGCAGGGTCCGAGG3’
cavPor3-miR-novel-chrscaffold-76-32980	GSP: 5’CGACATTGCCTAAGCCAGGGATT3’
	R: 5’ATCCAGTGCAGGGTCCGAGG3’

GSP is the specific primer which is matched to target gene; R is the primer that is matched to reverse transcription primer (R).

Table 3 Comparison of the data of anterior chamber, crystalline lens thickness, vitreous length, axial length, and refraction before and after lens-induced myopia in guinea pigs

LIM	Eye	Anterior chamber depth (Mean ± SEM, mm)	Crystalline lens thickness (Mean ± SEM, mm)	Vitreous length (Mean ± SEM, mm)	Axial length (Mean ± SEM, mm)	Refraction (Mean ± SEM, D)
Before	Fellow	1.25±0.05	3.39±0.09	3.58±0.17	8.23±0. 02	3.15±0.14
	LIM	1.27±0.04	3.41±0.11	3.55±0.11	8.24±0.03	3.23±0.22
After	Fellow	1.26±0.03	3.61±0.08	3.62±0.14	8.49±0.03	1.85±0.20
	LIM	1.28±0.07	3.63±0.06	3.74±0.12**	8.65±0.03**	-2.16±0.20**

Note: Compared with the relative LIM fellow, **P<0.0001. LIM: lens-induced myopia.

Figures

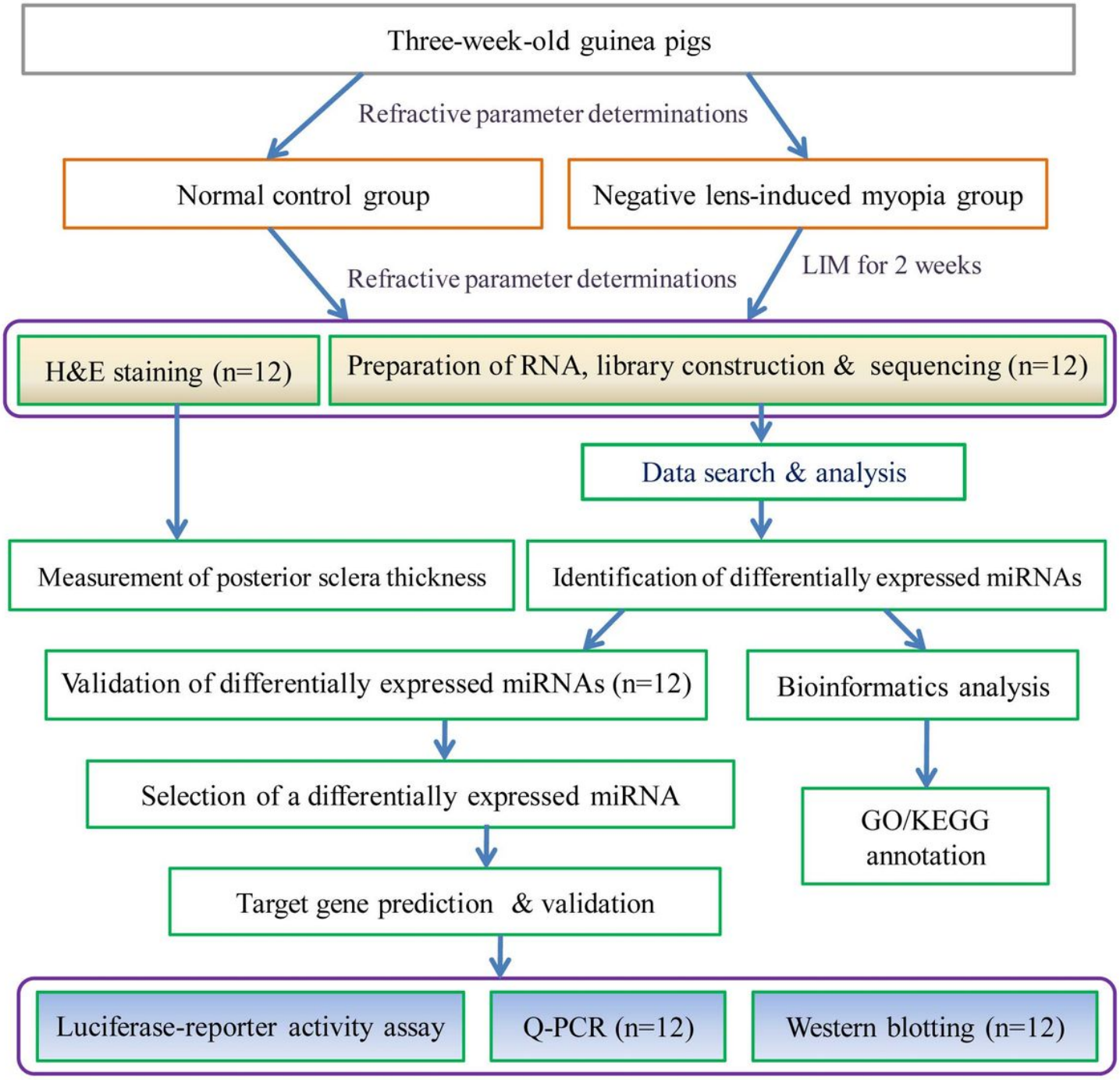

Figure 1

General design and workflow of the experiment. The determination at each stage includes normal control and lens-induced myopia groups, and each group contains six guinea pigs.

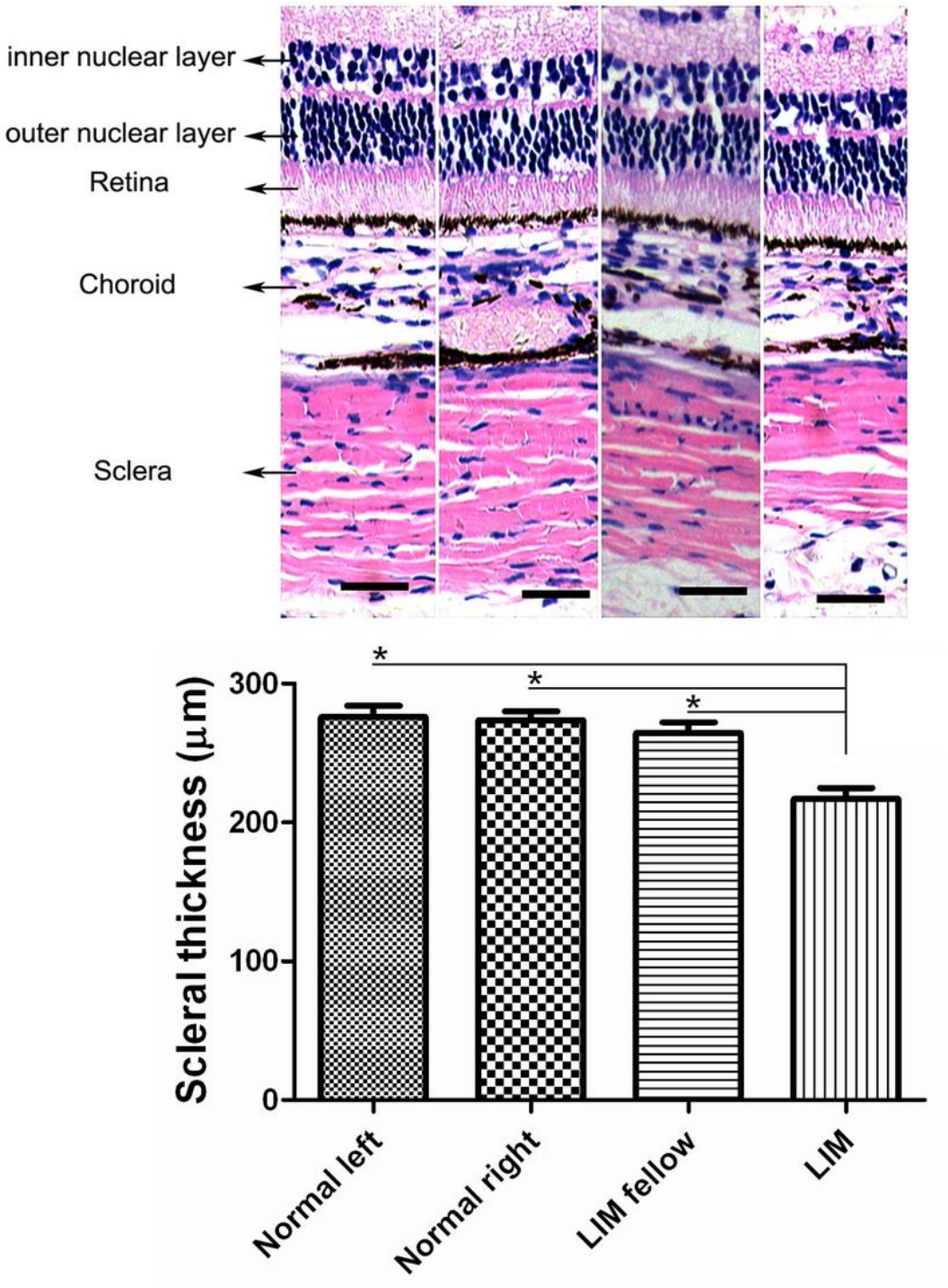

Figure 2

Alterations of the thickness of posterior sclera in normal control and LIM guinea pigs. After 2-week induction, eyeballs were extracted and fixed in 4% paraformaldehyde solution, and then the sections were cut and were stained with hematoxylin and eosin solutions (upper). Quantitative analysis of the scleral thickness in both control and LIM groups were performed (n = 6 for each group) and statistical analysis

was done (lower). a= normal left eye, b= normal right eye, c= LIM fellow eye, and d= LIM eye. Bar = 100 μm. *P < 0.01.

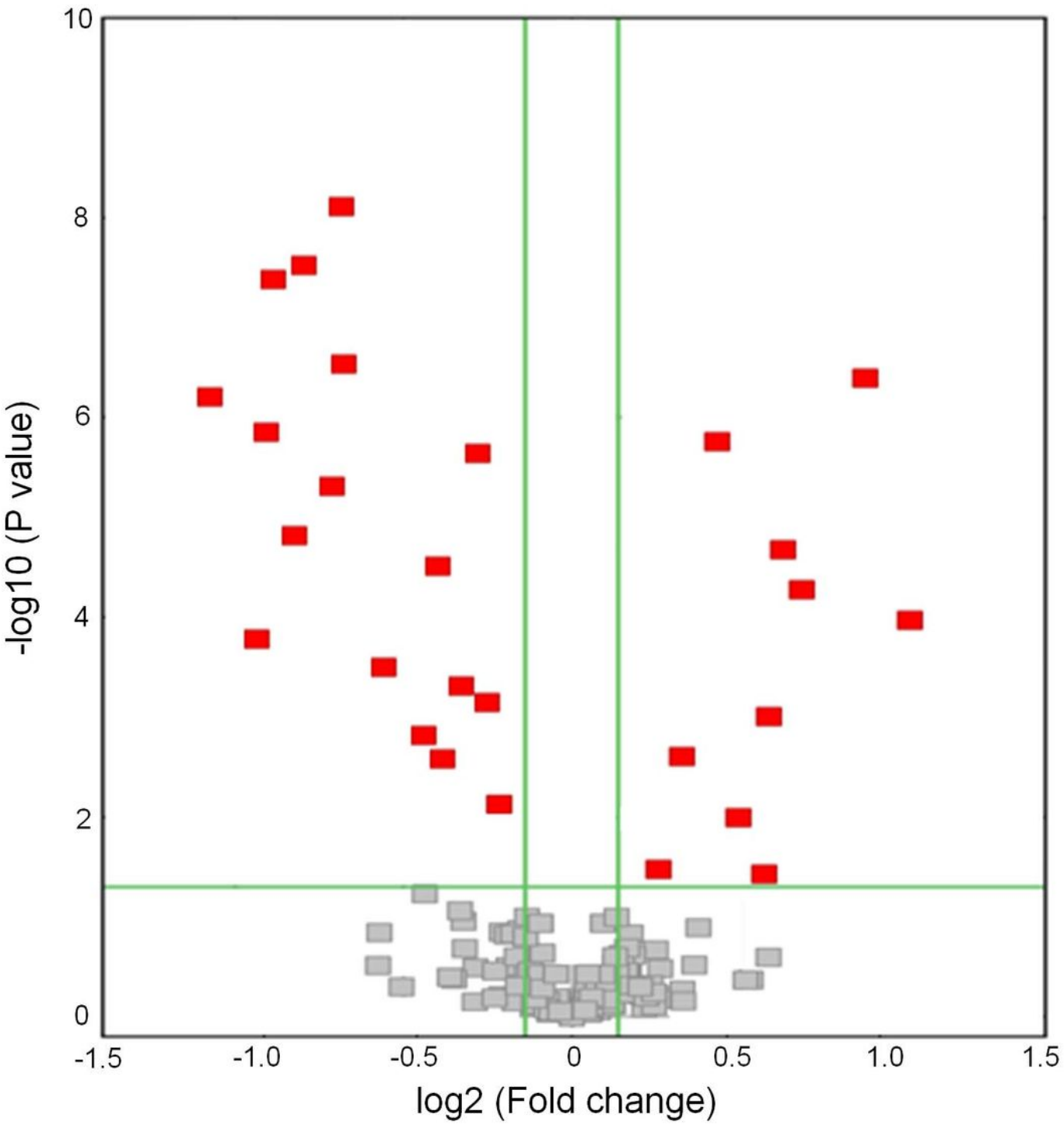

Figure 3

Volcano plot of differentially expressed microRNAs in lens-induced myopia sclera of guinea pigs. The red blocks are the differentially expressed microRNAs.

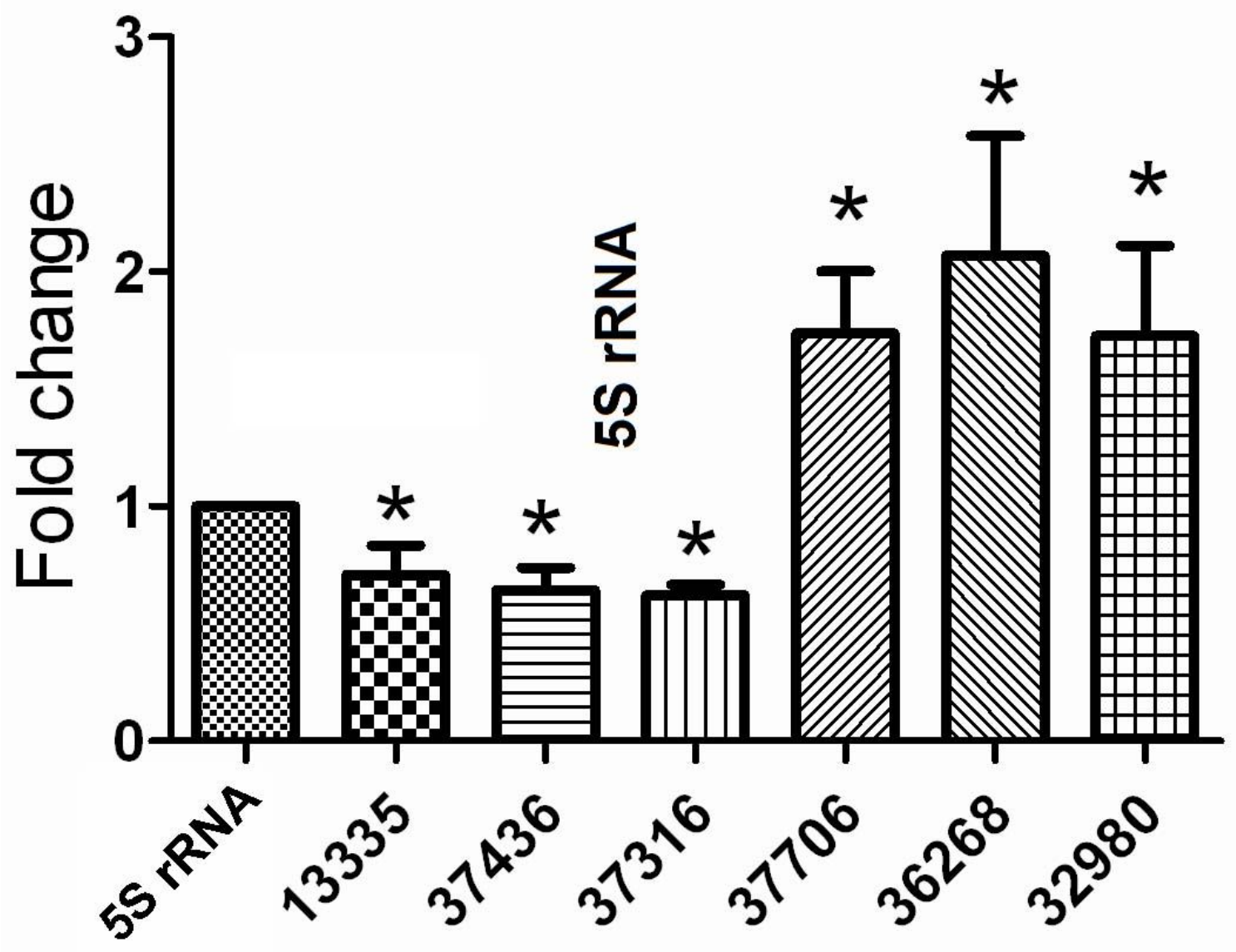

Figure 4

Validation of differentially expressed miRNAs in LIM guinea pig sclera by using quantitative PCR technique. Triplicate assays were performed for each RNA sample and the relative amount of each miRNA was normalized to 5S RNA. Statistically significant difference between LIM eyes and fellow subjects was presented by *P < 0.05 (n = 6). 13335= cavPor3-miR-novel-chrscaffold-13-13335, 37436= cavPor3-miR-novel-chrscaffold-120-37436, 37316= cavPor3-miR-novel-chrscaffold-119-37316, 37706= cavPor3-miR-novel-chrscaffold-128-37706, 36268= cavPor3-miR-novel-chrscaffold-107-36268, 32980= cavPor3-miR-novel-chrscaffold-76-32980.

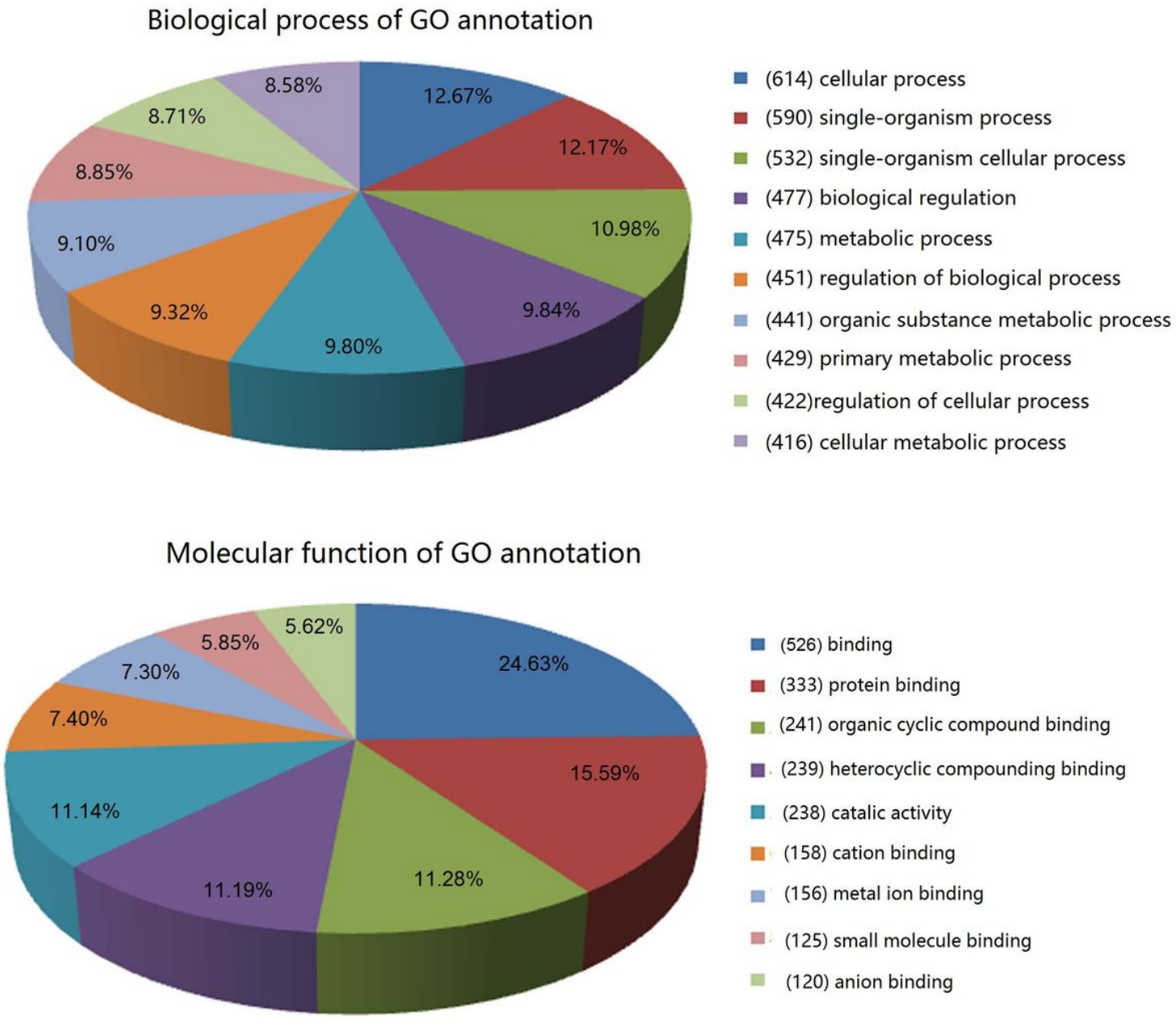

Figure 5

Annotations of differentially expressed microRNAs by GO annotation. Categorization of microRNA-targeted genes was performed according to the biological process and molecular function. The digit in the bracket is the number of differentially expressed genes associated with the GO term.

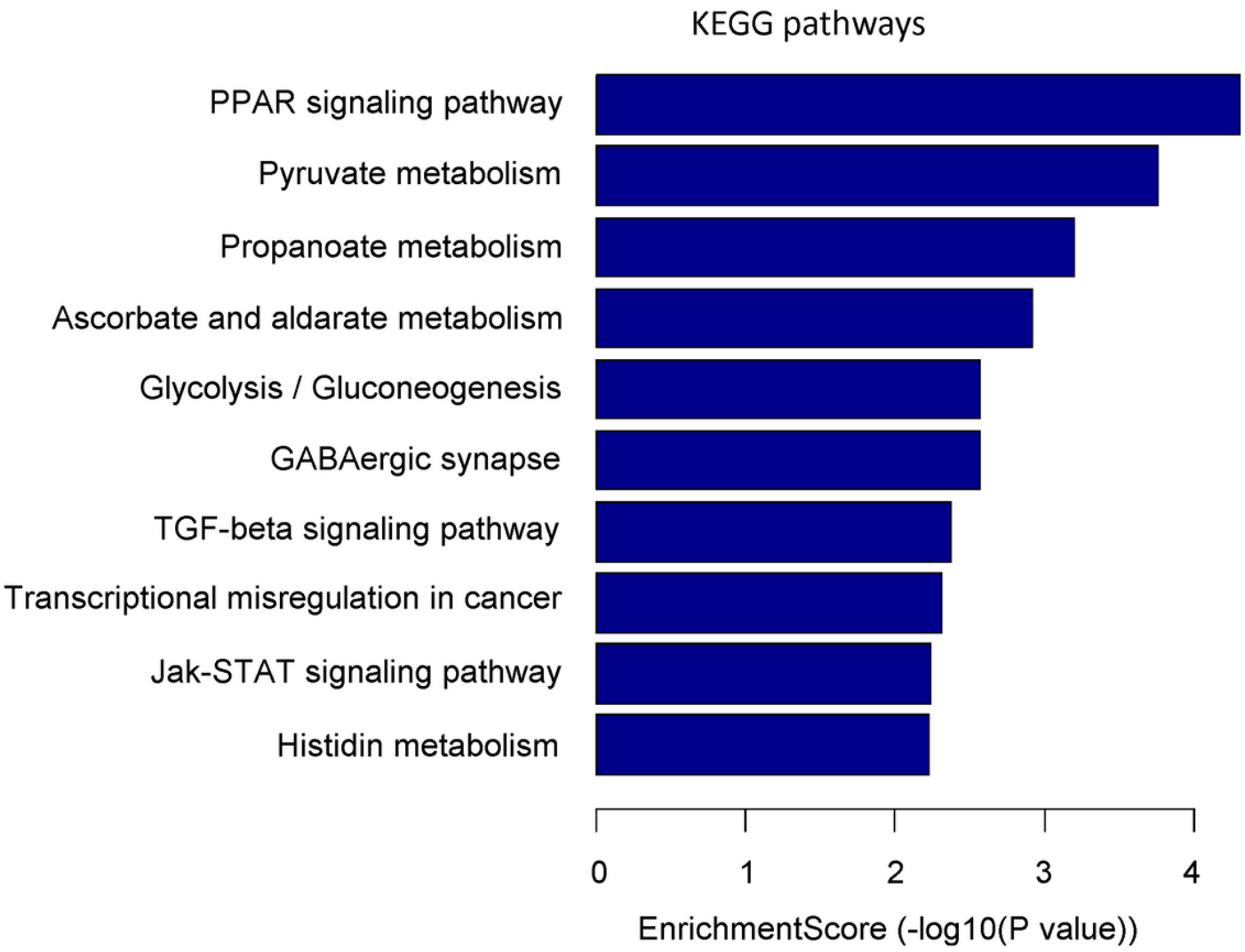

Figure 6

KEGG pathway enrichment analysis based on mRNAs targeted by differentially expressed miRNAs. Top ten signaling pathways are listed by the categorization.

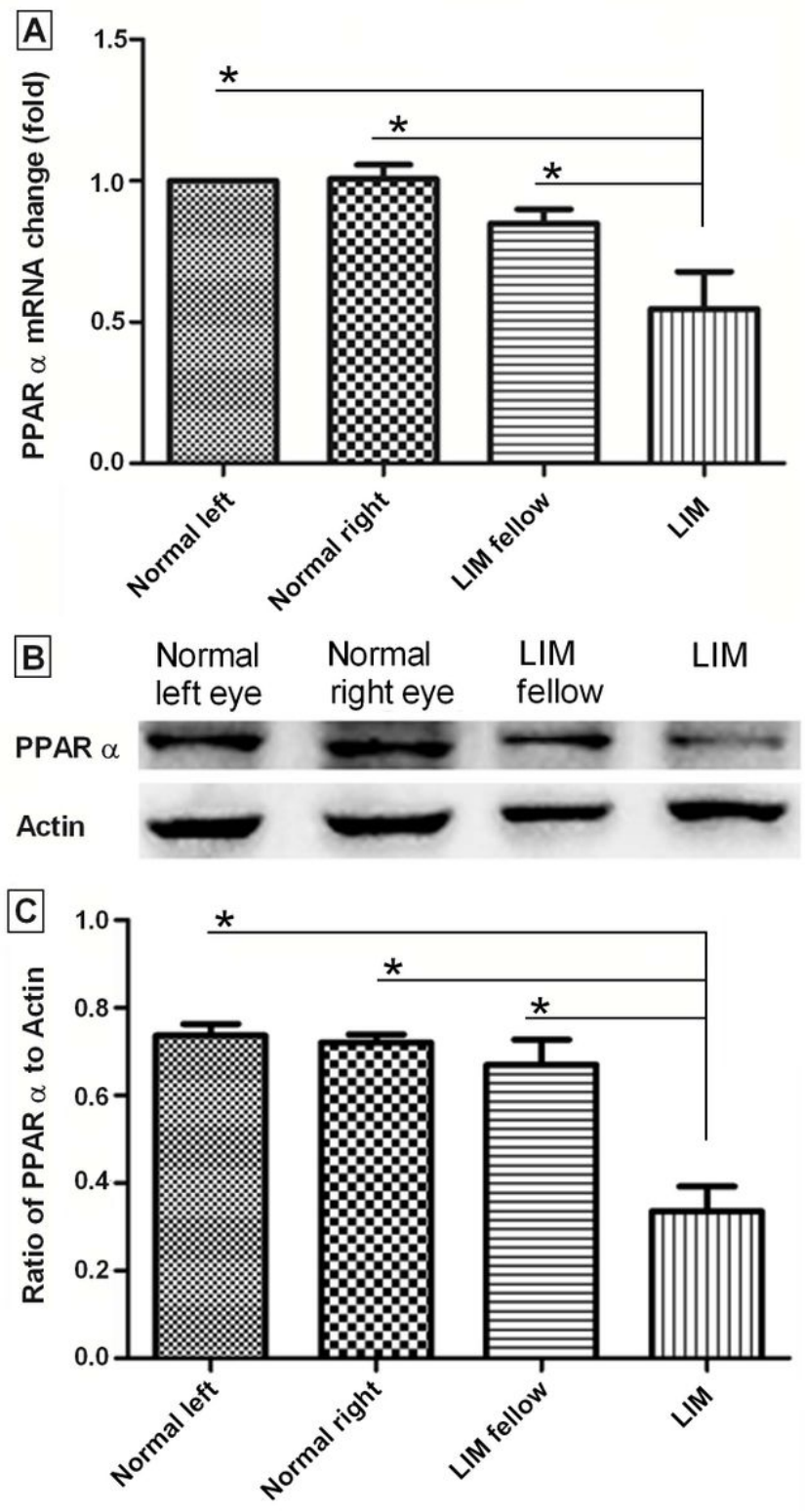

Figure 7

Determination of PPAR α at mRNA and protein levels in normal control and LIM guinea pig sclera. Using pooled samples, quantitative PCR (A) and western blotting (B) analyses were done, and histogram analysis was carried out for western blotting (C). Data were presented as mean ± SD for mRNA and protein expressions (n=6 for each group) and *P < 0.05.

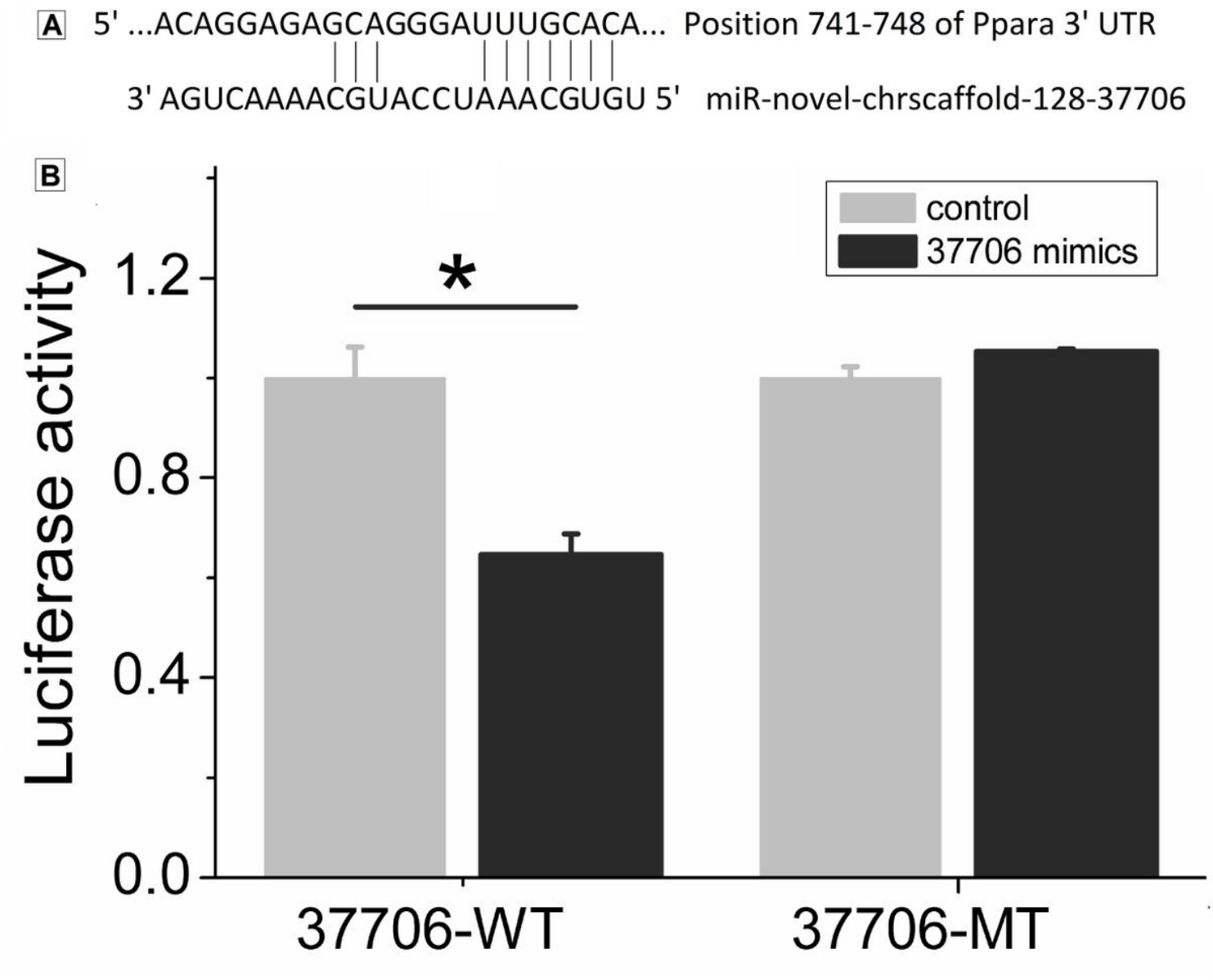

Figure 8

miR-novel-chrscaffold-128-37706 targeted PPAR α. (A) the sequence of 3’-UTR where PPAR α mRNA bound to miR-novel-chrscaffold-128-37706; (B) dual-luciferase reporter gene assay, which showed that miR-novel-chrscaffold-128-37706 mimics could inhibit the luciferase activity of miR-novel-chrscaffold-128-37706/PPAR α-WT plasmid. However, it had no effect on the luciferase activity of miR-novel-chrscaffold-128-37706/PPAR α-MT. *P < 0.05; WT, wild type; MT, mutant type.

Supplementary Files

This is a list of supplementary files associated with this preprint. Click to download.

- supplement1.docx